Properties of the negative effective magnetic pressure instability

K. Kemel[1,2]**, A. Brandenburg**[1,2]**, N. Kleeorin**[3]**, I. Rogachevskii**[3]

[1] NORDITA, AlbaNova University Center, Roslagstullsbacken 23, SE 10691 Stockholm, Sweden
[2] Department of Astronomy, AlbaNova University Center, Stockholm University, SE 10691 Stockholm, Sweden
[3] Department of Mechanical Engineering, The Ben-Gurion University of the Negev, POB 653, Beer-Sheva 84105, Israel

As was demonstrated in earlier studies, turbulence can result in a negative contribution to the effective mean magnetic pressure, which, in turn, can cause a large-scale instability. In this study, hydromagnetic mean-field modelling is performed for an isothermally stratified layer in the presence of a horizontal magnetic field, and the negative effective magnetic pressure instability (NEMPI) is comprehensively investigated. It is shown that, if the effect of turbulence on the mean magnetic tension force vanishes, which is consistent with results from direct numerical simulations of forced turbulence, the fastest growing eigenmodes of NEMPI are two-dimensional. The growth rate is found to be sensitive to details of the dependence of the effective mean magnetic pressure on the mean magnetic field. A fit formula is proposed that gives the growth rate as a function of turbulent kinematic viscosity, turbulent magnetic diffusivity, mean magnetic field strength, and the degree of stratification. The formation of sunspots and solar active regions is discussed as a possible application of NEMPI.

1 Introduction

The concept of turbulent viscosity is often used in astrophysical and other applications in recognition of the fact that the microscopic viscosity is far too small to be relevant on the length scales under consideration. Turbulent viscosity is the simplest parameterization of the Reynolds stress tensor, $\overline{u_i u_j}$, where $\boldsymbol{u} = \boldsymbol{U} - \overline{\boldsymbol{U}}$ is the velocity fluctuation about a suitably defined average, denoted here by an overbar. Turbulent viscosity is by far not the only contribution to the Reynolds stress tensor.

In addition to hydrodynamic contributions such as the Λ effect (Rüdiger 1980, 1989), which is relevant to explaining stellar differential rotation (Rüdiger & Hollerbach 2004), and the anisotropic kinetic alpha effect (Frisch et al. 1987), which provides an important test case in mean-field hydrodynamics (Brandenburg & von Rekowski 2001; Courvoisier et al. 2010), there are magnetic contributions as well. One can think of them as a magnetic feedback on the hydrodynamic stress tensor (Rädler 1974; Rüdiger 1974) or, especially when magnetic fluctuations are also considered, as a mean-field contribution to the turbulent Lorentz force.

Work by Rüdiger et al. (1986) suggested that the total magnetic tension force that includes the effects of fluctuations should be reduced and might even change sign. A similar result was obtained by Kleeorin et al. (1989, 1990) using spectral τ approach who also found another effect of a reversal of the effective magnetic pressure term; see also Kleeorin & Rogachevskii (1994) and Kleeorin et al. (1993, 1996). Rogachevskii & Kleeorin (2007) argued that in turbulent convection this can lead to the formation of large-scale magnetic flux structures and perhaps even sunspots and active regions.

Recently, direct numerical simulations (DNS) of both unstratified and stratified forced turbulence (Brandenburg et al. 2010, 2011; hereafter referred to as BKR and BKKR, respectively) have substantiated this idea and have demonstrated that the effective magnetic pressure can indeed change sign. Similar results have now also been obtained for turbulent convection (Käpylä et al. 2011a). These papers have provided mean-field calculations illustrating that there is a negative effective magnetic pressure instability (hereafter referred to as NEMPI) when there is sufficient density stratification.

This instability is the convective type instability as well as interchange instability in plasma (Tserkovnikov 1960; Priest 1982) or magnetic buoyancy instability (Parker 1966). On the other hand, the source of free energy of NEMPI is provided by the small-scale turbulence, while the free energy in interchange or magnetic buoyancy instability is drawn from the gravitational field. The mechanism of NEMPI works even under isothermal conditions when entropy evolution is ignored and an isothermal equation of state is used. Three-dimensional calculations have shown that the mean magnetic field develops structure along the direction of the field (BKR). However, while the mean-field calculations have illustrated the nature of the instability, no systematic survey of solutions has yet been attempted.

The purpose of this paper is to clarify some still puzzling aspects concerning NEMPI. This is particularly important in view of the fact that no clear evidence of NEMPI has yet been seen in DNS (BKKR). In other words, although DNS

have shown that the effective mean magnetic pressure can change sign, and although we know from mean-field models that this should lead to the formation of structures near the surface, this type of structure formation has not been seen in DNS.

On the other hand, some type of structure formation has recently been reported in Large-Eddy Simulations (LES), so one wonders whether this might be an indication of NEMPI. We have here in mind the radiation magneto-convection simulations of Kitiashvili et al. (2010), in which one sees the formation of whirlpool-like magnetic structures. However, even in the absence of magnetic fields, one finds the formation of whirlpools, although this requires rapid rotation (Käpylä et al. 2011b).

Most relevant to NEMPI is perhaps the work of Tao et al. (1998), who also considered magneto-convection and find a horizontal segregation into magnetized and non-magnetized regions. The size of the individual regions is such that they encompass several turbulent eddies. This phenomenon might therefore well be associated with an effect that could also be modelled in terms of mean-field theory. However, before we can make such an association, we need to find out more about the properties of NEMPI. In particular, we need to know what is the optimal magnetic field strength, what are the requirements or restrictions in the turbulent velocity, and, finally, how much density stratification is needed to make NEMPI work.

To connect the aforementioned requirements to DNS, we need to have a meaningful parameterization of the turbulence effects. The work done so far has been focussing on measuring a reduction of the turbulent pressure and effective mean magnetic pressure as a function of the local mean magnetic field strength. The shape of the resulting dependence of the effective mean magnetic pressure on the mean magnetic field has been matched to a specific fit formula that can be characterized by two fit parameters that, in turn, can be linked to the minimum effective mean magnetic pressure and the critical field strength above which the effect is suppressed. However, there have been indications that this parameterization is not unique and that different combinations of the two fit parameters can result in similar values of minimum effective pressure and the critical field strength. The question therefore arises whether this degeneracy is important for the properties of NEMPI.

Finally, we mentioned already the fact that NEMPI is capable of exciting three-dimensional structures that show variation along the direction of the mean magnetic field. This would raise the worry that the two-dimensional results presented so far may not reflect the properties of the fastest growing mode and may therefore not be relevant to describing NEMPI. However, it turns out that this is not the case, because the degree to which three-dimensional modes are excited depends on the sign of one of the turbulence parameters, namely the term characterizing turbulence effects on the magnetic tension force, and that simulations indicate that this sign is not favorable for exciting three-

dimensional modes (BKR). Before we begin addressing the various points, we discuss first the mean-field model and turn then to the points raised above.

2 Mean-field model

In view of future verifications of NEMPI with DNS, it is essential to be able to reduce the essential physics to a minimum. We will therefore not make any attempt to consider other aspects that would make the model more realistic with respect to the Sun. Given that NEMPI works even under isothermal conditions (BKKR), we adopt an isothermal equation of state where the mean pressure $\overline{p}$ is linear in the mean density $\overline{\rho}$, with $\overline{p} = \overline{\rho} c_{\mathrm{s}}^2$, and $c_{\mathrm{s}} = \mathrm{const}$ being the isothermal sound speed. We solve the evolution equations for mean velocity $\overline{U}$, mean density $\overline{\rho}$, and mean vector potential $\overline{A}$, in the form

$$\frac{\partial \overline{U}}{\partial t} = -\overline{U} \cdot \nabla \overline{U} - c_{\mathrm{s}}^2 \nabla \ln \overline{\rho} + g + \overline{\mathcal{F}}_{\mathrm{M}} + \overline{\mathcal{F}}_{\mathrm{K}}, \quad (1)$$

$$\frac{\partial \overline{\rho}}{\partial t} = -\overline{U} \cdot \nabla \overline{\rho} - \overline{\rho} \nabla \cdot \overline{U}, \quad (2)$$

$$\frac{\partial \overline{A}}{\partial t} = \overline{U} \times \overline{B} - (\eta_{\mathrm{t}} + \eta) \overline{J}, \quad (3)$$

where $\overline{\mathcal{F}}_{\mathrm{M}}$ is given by

$$\overline{\rho} \, \overline{\mathcal{F}}_{\mathrm{M}} = -\tfrac{1}{2} \nabla[(1 - q_{\mathrm{p}}) \overline{B}^2] + \overline{B} \cdot \nabla \left[(1 - q_{\mathrm{s}}) \overline{B} \right], (4)$$

and

$$\overline{\mathcal{F}}_{\mathrm{K}} = (\nu_{\mathrm{t}} + \nu) \left(\nabla^2 \overline{U} + \nabla \nabla \cdot \overline{U} + 2 \overline{\mathsf{S}} \nabla \ln \overline{\rho} \right) \quad (5)$$

is the total (turbulent plus microscopic) viscous force. Here, $\mathsf{S}_{ij} = \tfrac{1}{2}(\overline{U}_{i,j} + \overline{U}_{j,i}) - \tfrac{1}{3} \delta_{ij} \nabla \cdot \overline{U}$ is the traceless rate of strain tensor of the mean flow. As in earlier work (BKR, BKKR), we approximate q_{p} and q_{s} by simple profiles that are only functions of the ratio $\beta \equiv |\overline{B}|/B_{\mathrm{eq}}$, i.e.,

$$q_{\sigma}(\beta) = q_{\mathrm{i}0}[1 - (2/\pi) \arctan(\beta^2/\beta_{\sigma}^2)], \quad (6)$$

where σ stands for subscripts p and s, respectively. The functions q_{p} and q_{s} quantify the impact of the mean magnetic field on the effective pressure and tension forces, respectively.

As initial condition, we assume a hydrostatic stratification with $\overline{\rho}(z) = \rho_0 \exp(-z/H_{\rho})$, where $H_{\rho} = c_{\mathrm{s}}^2/g$ is the scale height in a domain of size $L_x \times L_y \times L_z$, where $-L_z/2 \leq z \leq L_z/2$. We normally use $L_x = L_y \equiv L$ and, unless noted otherwise, also $L_z = L$. In most of the cases we use $L_x = L_y = L_z \equiv L$. We add a small perturbation to the velocity field. We allow for the presence of an imposed field in the y direction, $B_0 = (0, B_0, 0)$. The total field is then written as

$$\overline{B} = B_0 + \nabla \times \overline{A}, \quad (7)$$

so the departure from the imposed field is expressed in terms of the mean magnetic vector potential $\overline{A}$.

On the upper and lower boundaries we adopt stress-free boundary conditions for velocity, i.e. $\overline{U}_{x,z} = \overline{U}_{y,z} = \overline{U}_z =$
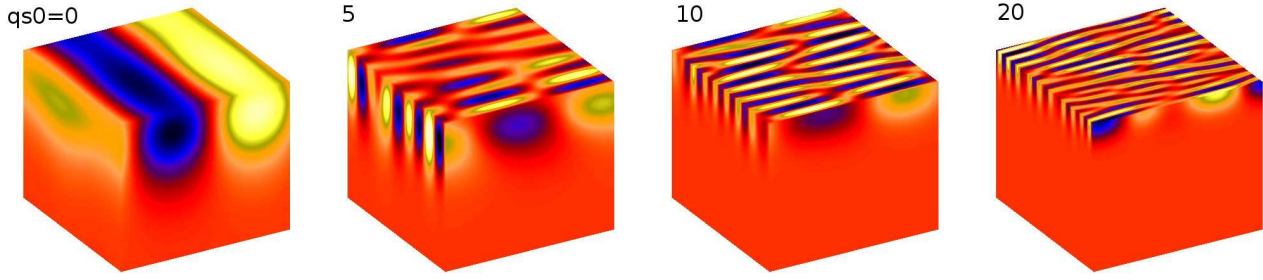
Fig. 1   Visualization of $\overline{B}_y$ at the periphery of the computational domain near the end of the kinematic growth phase. Note the change of the field pattern with increasing values of q_{s0} (=0, 5, 10, and 20 from left to right).

0, and a perfect conductor boundary condition for the magnetic field, i.e. $\overline{A}_x = \overline{A}_y = \overline{A}_{z,z} = 0$. Here, commas denote partial differentiation. No boundary condition for the density is required. All computations have been carried out with the PENCIL CODE[1].

Our model is characterized by the following set of input parameters. There are four parameters characterizing the hydrostatic equilibrium stratification, namely g, c_s^2, ρ_0, and L_z. The remaining parameters are the Alfvén speed at the surface, $v_A^{top} = B_0/\sqrt{\rho_{top}\mu_0}$, turbulent viscosity and magnetic diffusivity, as well as the parameters $q_{\sigma0}$ and β_σ. Here, $\rho_{top} = \rho_0 \exp(-z_{top}/H_\rho)$ is the density at the surface, which is usually at $z \equiv z_{top} = L_z/2$.

3   Results

3.1   Two- and three-dimensional solutions

Earlier work has suggested that the eigenmodes of NEMPI can be three-dimensional (BKR). This could make two-dimensional calculations questionable if the first excited mode were indeed the fastest growing one. However, it turns out that the wavelength of the eigenmode in the direction of the field increases as q_s decreases. In BKR, where three-dimensional (y-dependent) solutions to NEMPI were first reported, q_s was chosen to be around 10, and the fastest growing mode was indeed three-dimensional. In Fig. 1 we show that the effective wavenumber of the variation of the field in the y direction decreases with decreasing values of q_s. This is shown quantitatively in Fig. 2, where we plot the dependence of the typical value of the field-aligned wavenumber, k_y, on the value of q_{s0}. Here, k_y is evaluated in a layer near the surface. For normalization purposes, we define the lowest wavenumber in the computational domain as $k_1 = 2\pi/L$.

We find that the typical value of k_y grows approximately linearly with increasing values of q_{s0}. As an approximate fit formula we can use $k_y^2/k_1^2 \approx 1.3\, q_{s0}$. In addition, we find that the growth rate of the instability, λ, grows with q_{s0} approximately linearly, once q_{s0} exceeds a value of around 5. The fact that $k_y \to 0$ as $q_{s0} \to 0$ is significant, because

BKKR and also Käpylä et al. (2011b) found from simulations that $q_{s0} \approx 0$. In that case, the characteristic length scale along the direction of the field becomes infinite and the calculation essentially two-dimensional. Conversely, when studying NEMPI in two dimensions, changing the value of q_{s0} has no effect on structure formation and the growth rate; see Table 1. However, it is now clear that this is an artifact of restricting the solutions to be two-dimensional.

3.2   Degeneracy in the q_p fit formula

We mentioned in the introduction that recent attempts to determine q_{p0} from simulations faced the difficulty that the fit formula possesses a degeneracy in that we can obtain a similarly looking dependence of the effective mean magnetic pressure $\mathcal{P}_{eff}(\beta) = [1 - q_p(\beta)]\,\beta^2$ over a wide range of values of q_{p0} by adjusting the value of β_p correspondingly. The core of the problem becomes clear from Fig. 3, where we plot the function $\mathcal{P}_{eff}(\beta)$ in the lower panel and $\min(\mathcal{P}_{eff})$ versus β_{crit} in the upper panel. The parameter β_{crit} is defined by the condition $\mathcal{P}_{eff}(\beta_{crit}) = 0$. It is evident that $\min(\mathcal{P}_{eff})$ becomes more negative as β_{crit} decreases and q_{p0} increases. However, for a given value of β_{crit}, the fit formula cannot produce a minimum of $\mathcal{P}_{eff}$ that is below a certain value. This minimum value is attained for $q_{p0} \to \infty$, but even the graphs for $q_{p0} = 50$ or 20 lie quite close together. Conversely, for a given value of $\min(\mathcal{P}_{eff})$, there is a minimum value of β_{crit} below which there is no solution. For $\min(\mathcal{P}_{eff}) = -0.1$, for example, there are no values of q_{p0} for β_{crit} below about 0.3, while between 0.30 and 0.35 the same value of $\min(\mathcal{P}_{eff})$ can be attained for q_{p0} between 20 and ∞. This is shown more clearly in the second panel of

Table 1   Comparison of growth rates for different values of L_y and q_s, including a two-dimensional (2D) simulation ($L_y \to \infty$).

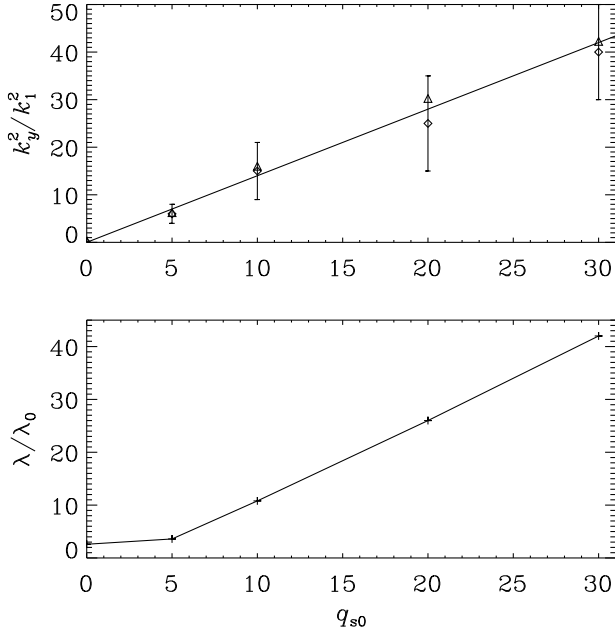|	L_y	$q_s = 0$	$q_s = 30$
3D	L	0.0124	0.2070
3D	$8L$	0.0137	
2D	∞	0.0141	0.0141

---

[1]   http://www.pencil-code.googlecode.com

Fig. 2 Dependence of k_y on q_{s0} (upper panel), together with the corresponding growth rate λ (lower panel). Here, λ is normalized by $\lambda_0 \equiv g/c_s$.

Fig. 3, where we plot $\mathcal{P}_{eff}(\beta)$ for different values of q_{p0} and values of β_{crit} that all cross the line $\min(\mathcal{P}_{eff}) = -0.1$ in the upper panel of this figure. This shows that, when q_{p0} is 10 or larger, the graph of $\mathcal{P}_{eff}(\beta)$ becomes quite insensitive to the exact value of q_{p0}, and that the same graphs can be obtained for a set of different combinations of q_{p0} and β_p.

In the family of similarly looking solutions, the optimal value of B_p is found to decrease with increasing values of q_{p0}, as is shown in the upper panel of Fig. 4. However, even though the graphs of $q_p(\beta)$ are rather similar, mean-field simulation show that the resulting growth rates are sensitive to the value of q_p in the parameter regime where $\overline{B}/B_{eq}$ is small. An alternative would be to use a third observation to fix the degeneracy of the model. One such parameter could be the position of the minimum of $\mathcal{P}_{eff}$, i.e., the value β_{min}, for which $\mathcal{P}_{eff}(\beta_{min}) = \min(\mathcal{P}_{eff})$ is obeyed.

3.3 Onset condition of NEMPI

With a given prescription of $q_p(\beta)$, assuming here $q_{s0} = 0$, we can now compute two-dimensional mean-field models. Our goal is to obtain a simple description that can tell us how large the growth rate of the instability is, and what the critical condition for the onset of the instability is. Not much is known about the linear stability properties of NEMPI, so we have to rely on numerical determinations of the growth rates for different wavelengths in the different directions to obtain an approximate representation of the dispersion relation. Earlier work of Kemel et al. (2011) has suggested a relation of the form

$$\lambda = \Phi(v_A^{top}, g/c_s^2, q_{p0}, \beta_{crit}) - \nu_t k_\nu^2 - \eta_t k_\eta^2, \tag{8}$$
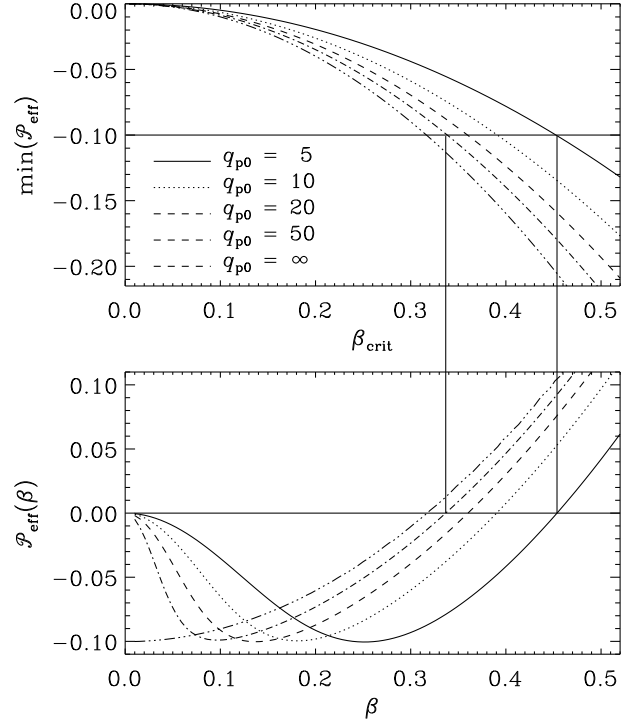

Fig. 3 Minimum effective magnetic pressure versus β_{crit} for 5 values of q_{p0} (upper panel), and the corresponding graphs of $\mathcal{P}_{eff}(\beta)$ for which $\mathcal{P}_{eff} = -0.1$. For two values of q_{p0} (5 and 50) the correspondence between β_{crit} and the zero point of $\mathcal{P}_{eff}(\beta)$ for curves with $\min(\mathcal{P}_{eff}) = -0.1$ is shown by vertical lines.

where k_ν and k_η are inverse length scales quantifying the effects of turbulent viscosity and turbulent magnetic diffusivity, Φ is a function of the Alfvén speed at the top, v_A^{top}, the inverse scale height $H_\rho^{-1} = g/c_s^2$, and other parameters describing the functional form of q_p.

We now need to determine the various unknowns. We begin by determining k_ν and k_η by varying either only ν_t or only η_t at a time. In this way we obtain a linear fit for the growth rate, $\lambda(\eta_t) = \text{const} - \eta_t k_\eta^2$, giving us k_η^2 as the slope of this graph; see the upper and lower panels of Fig. 5 for the corresponding results for k_ν and k_η, respectively. It turns out that $k_\nu \approx 0.77\,k_1$ and $k_\eta \approx 1.1\,k_1$. The surprising result is that k_ν and k_η are different from each other by a factor of about $\sqrt{2}$. This was not the case in the earlier work of Kemel et al. (2011) using less accurate data. The new data seem sufficiently accurate so that this discrepancy cannot easily be explained by numerical errors. More plausibly, this discrepancy could be explained by a residual dependence of Φ on either ν_t or η_t, or both. Note, however, that the turbulent magnetic Prandtl number is of order unity (Kleeorin & Rogachevskii 1994; Yousef et al. 2003), so this uncertainty should be of no practical relevance.

Accepting now the fit parameters k_ν and k_η as they have been measured, we can proceed to determining the dependence of Φ on v_A^{top}, H_ρ, and other fit physical input param-
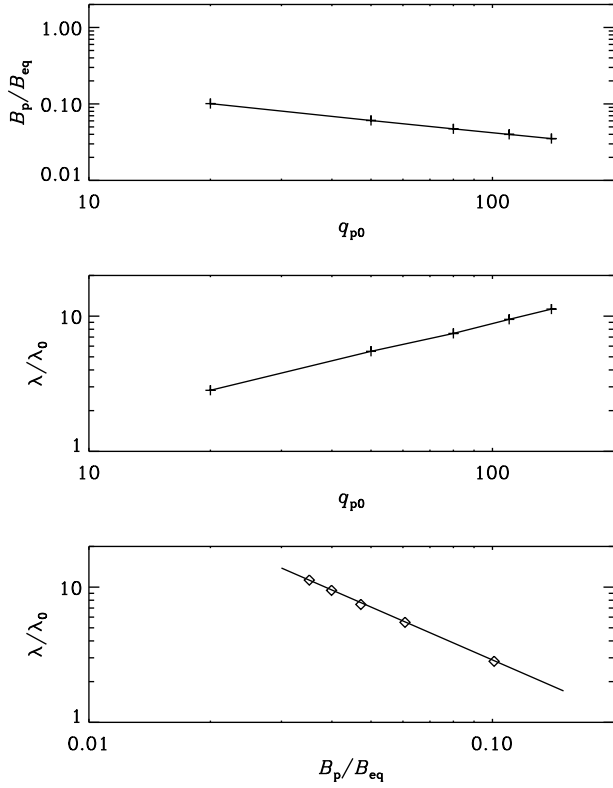
Fig. 4 Dependence of the fit parameter B_{p} on q_{p0}, the corresponding growth rate λ, and the dependence of λ on B_{p}. Here, λ is normalized by $\lambda_0 \equiv g/c_{\mathrm{s}}$.

Fig. 5 Dependence of λ on η_{t} (upper panel) and ν_{t} (lower panel). In the two panels, the straight lines represent the negative slopes $k_{\eta}^2 \approx 1.2$ and $k_{\nu}^2 \approx 0.6$, approximately. In the lower panel, the dotted line gives, for comparison, the negative slope 1.2 of the upper panel.

eters. We assume that this relation is multiplicative and find first the dependence on $v_{\mathrm{A}}^{\mathrm{top}}$ by plotting $\Phi = \lambda + \nu_{\mathrm{t}} k_{\nu}^2 + \eta_{\mathrm{t}} k_{\eta}^2$ against $v_{\mathrm{A}}^{\mathrm{top}}$. It turns out that this is nearly a linear relationship. Thus, keeping all other parameters unchanged, we find Φ as a function of $v_{\mathrm{A}}^{\mathrm{top}}$; see the first panel of Fig. 6. Next, we find Φ as a function of g/c_{s}^2, which results in an exponential relationship, where $\ln \Phi$ is found to increase linearly with $g/c_{\mathrm{s}}^2 \equiv H_{\rho}^{-1}$; see the middle panel of Fig. 6. Thus, we can write $\ln \Phi \propto 1/k_{\rho}H_{\rho}$, where k_{ρ} is a new fit parameter. Here, $k_{\rho} \approx 0.5\, k_1$. Finally, we show in the third panel of Fig. 6 the dependence of Φ on the reconstructed fit,

$$\Phi_{\mathrm{fit}} = v_{\mathrm{A}}^{\mathrm{top}} k_{\mathrm{A}} \exp(1/k_{\rho}H_{\rho})\, \varphi(q_{\mathrm{p0}}, \beta_{\mathrm{p}}), \qquad (9)$$

where $k_{\mathrm{A}} \approx 0.26\, k_1$ gives the best fit. This combined fit appears reasonably accurate for most of the parameter regime, substantiating thus the general validity of the fit formulae (8)–(9).

Some comments about the system size are in order. In all cases with $q_{\mathrm{s0}} = 0$, we find that in three-dimensional calculations with finite y extent, the value of L_y affects the growth rates only slightly; see Table 1. On the other hand, doubling the x extent yields two pairs of rolls, but at a slightly lower growth rate, indicating that our standard value of L_x is still not quite in the asymptotic regime. Extending the domain downward (in the negative z direction)
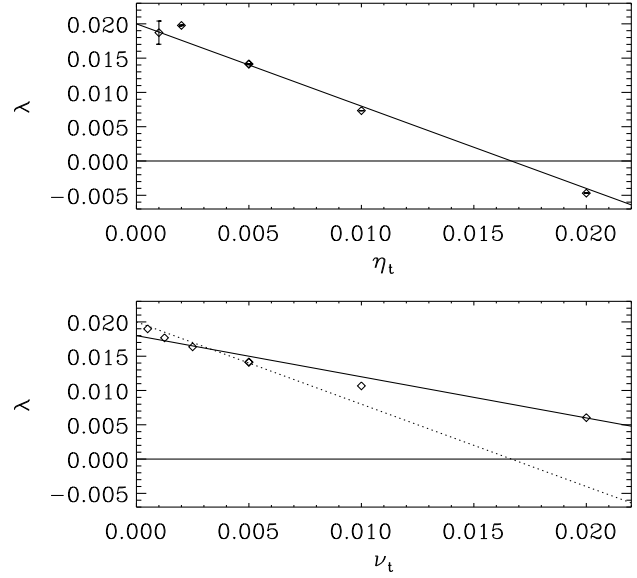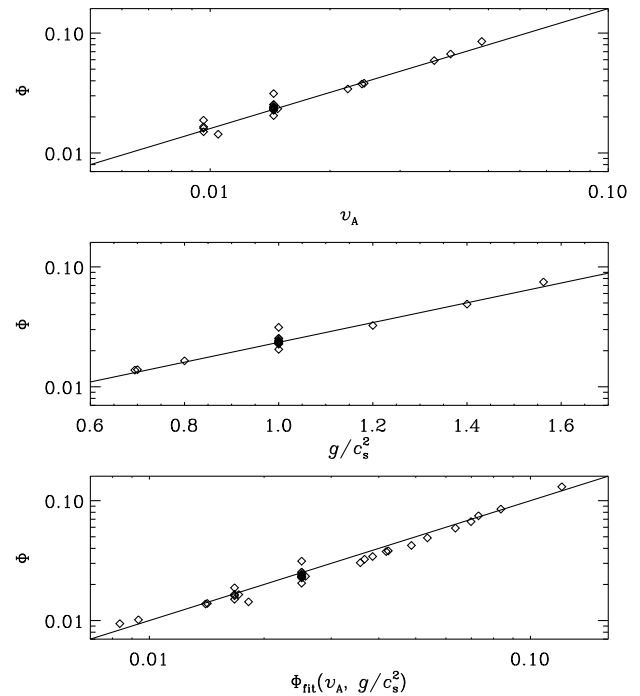

Fig. 6 Dependence of $\tilde{\lambda}$ on $v_{\mathrm{A}}^{\mathrm{top}}$ (upper panel), g/c_{s}^2 (middle panel), and the combined fit $\Phi(v_{\mathrm{A}}^{\mathrm{top}}, g/c_{\mathrm{s}}^2)$ (lower panel).

does not change the results at all, but extending it in the upward direction (positive z direction) changes the value of

$\rho_{\rm top}$ and hence the value of $v_{\rm A}^{\rm top}$ in a way that is already fully described by our scaling law in Eq. (9).

4   Conclusions

The present work has clarified a number of puzzling aspects of NEMPI. Firstly, it is now clear that we can proceed with two-dimensional simulations as long as we know that $q_{\rm s0} = 0$ (or negative). However, this may not always be the case. The fact that three-dimensional structures can emerge from NEMPI was initially thought to be an interesting aspect, because it could readily explain the formation of bipolar regions (BKR). However, given that simulations now indicate that $q_{\rm s0} \approx 0$ (or perhaps even negative), this proposal would no longer be an option, unless some other as yet unexplored effect begins to play a role. In principle, all turbulent transport processes are nonlocal and must be described by a convolution with the mean field rather than a multiplication. In Fourier space, the convolution corresponds to a multiplication with a scale-dependent turbulent transport coefficient. Thus, the idea of explaining bipolar regions would again become viable if this effect only existed at intermediate length scales. This would be a task for future simulations to clarify, because none of the currently available techniques are yet equipped to addressing this possibility.

Next, we have seen that the degeneracy in the fit formula used for $q_{\rm p}(\beta)$ and $P_{\rm eff}(\beta)$ is significant in that different combinations of $q_{\rm p0}$ and $\beta_{\rm p}$ result in similar values of $\min(P_{\rm eff})$ and $\beta_{\rm crit}$, but the growth rates can still be quite different. This means that it is not sufficient to measure only $\min(P_{\rm eff})$ and $\beta_{\rm crit}$. Instead, to characterize the functional form of $P_{\rm eff}(\beta)$ more accurately, we need some other characteristics to represent the dependence of this function near the origin. One such possibility is to use the field strength for which the minimum of the effective magnetic pressure is reached.

Finally, we have tried to establish an approximate dispersion relation to predict the growth rate of NEMPI as a function of turbulent viscosity, turbulent magnetic diffusivity, mean field strength, and the strength of stratification. This formula may serve as a first orientation and can hopefully be improved further with future simulations. This formula can also be useful in connection with analytic estimates concerning the regimes when NEMPI is expected in DNS or under other more realistic circumstances.

References

Brandenburg, A., von Rekowski, B.: 2001, A&A 379, 1153
Brandenburg, A., Kleeorin, N., Rogachevskii, I.: 2010, AN 331, 5 (BKR)
Brandenburg, A., Kemel, K., Kleeorin, N., Rogachevskii, I.: 2011, ApJ (submitted), arXiv:1005.5700 (BKKR)
Courvoisier A., Hughes D. W., Proctor M. R. E.: 2010, Proc. Roy. Soc. Lond. 466, 583
Frisch, U., She, Z. S., Sulem, P. L.: 1987, Physica 28D, 382
Käpylä, P. J., Mantere, M. J., Hackman, T.: 2011a, ApJ (submitted), arXiv:1106.6029
Käpylä, P. J., Brandenburg, A., Kleeorin, N., Mantere, M. J., Rogachevskii, I.: 2011b, MNRAS (submitted), arXiv:1104.4541
Kemel, K., Brandenburg, A., Kleeorin, N., Rogachevskii, I.: 2011, in Proc. IAU, Vol. 6, IAU Symp. S274 (eds.), *Advances in Plasma Astrophysics*, A. Bonanno, E. de Gouveia dal Pino, A. Kosovichev, p. 473
Kitiashvili, I. N., Kosovichev, A. G., Wray, A. A., Mansour, N. N.: 2010, ApJ 719, 307
Kleeorin, N., Mond, M., Rogachevskii, I. 1993, Phys. Fluids B, 5, 4128
Kleeorin, N., Mond, M., Rogachevskii, I.: 1996, A&A 307, 293
Kleeorin, N., Rogachevskii, I.: 1994, PhRvE 50, 2716
Kleeorin, N.I., Rogachevskii, I.V., Ruzmaikin, A.A.: 1989, Sov. Astron. Lett. 15, 274
Kleeorin, N.I., Rogachevskii, I.V., Ruzmaikin, A.A.: 1990, Sov. Phys. JETP 70, 878
Parker, E.N.: 1966, ApJ 145, 811
Priest, E.R.: 1982, *Solar Magnetohydrodynamics* (D. Reidel Publ. Co., Dordrecht)
Rädler, K.-H.: 1974, AN 295, 265
Rogachevskii, I., Kleeorin, N.: 2007, PhRvE 76, 056307
Rüdiger, G.: 1974, AN 295, 275
Rüdiger, G.: 1980, GApFD 16, 239
Rüdiger, G.: 1989, *Differential rotation and stellar convection: Sun and solar-type stars* (Gordon & Breach, New York)
Rüdiger, G., Hollerbach, R.: 2004, *The magnetic universe* (New York: Wiley-VCH, Weinheim)
Rüdiger, G., Tuominen, I., Krause, F., Virtanen, H.: 1986, A&A 166, 306
Tao, L., Weiss, N.O., Brownjohn, D.P., Proctor, M.R.E.: 1998, ApJ 496, L39
Tserkovnikov, Y. A.: 1960, Sov. Phys. Dokl., 5, 87
Yousef, T. A., Brandenburg, A., Rüdiger, G.: 2003, A&A 411, 321